ELSEVIER

Journal of Structural Geology 29 (2007) 1512–1521

JOURNAL OF STRUCTURAL GEOLOGY

www.elsevier.com/locate/jsg

On the extent of size range and power law scaling for particles of natural carbonate fault cores

Andrea Billi*

Dipartimento di Scienze Geologiche, Università ''Roma Tre'', Largo S.L. Murialdo 1, 00146 Roma, Italy

Received 14 December 2006; received in revised form 11 May 2007; accepted 20 June 2007
Available online 19 July 2007

Abstract

To determine the size range and both type and extent of the scaling laws for particles of loose natural carbonate fault rocks, six granular fault cores from Mesozoic carbonate strata of central Italy were sampled. Particle size distributions of twelve samples were determined by combining sieving and sedimentation methods. Results show that, regardless of the fault geometry, kinematics, and tectonic history, the size of fault rock particles respects a power law distribution across approximately four orders of magnitude. The fractal dimension (D) of the particle size distribution in the analysed samples ranges between $\sim$2.0 and $\sim$3.5. A lower bound to the power law trend is evident in all samples except in those with the highest D-values; in these samples, the smallest analysed particles ($\sim$0.0005 mm in diameter) were also included in the power law interval, meaning that the lower size limit of the power law distribution decreases for increasing D-values and that smallest particles start to be comminuted with increasing strain (i.e. increasing fault displacement and D-values). For increasing D-values, also the largest particles tends to decrease in number, but this evidence may be affected by a censoring bias connected with the sample size. Stick-slip behaviour is suggested for the studied faults on the basis of the inferred particle size evolutions. Although further analyses are necessary to make the results of this study more generalizable, the preliminary definition of the scaling rules for fault rock particles may serve as a tool for predicting a large scale of fault rock particles once a limited range is known. In particular, data from this study may result useful as input numbers in numerical models addressing the packing of fault rock particles for frictional and hydraulic purposes.

Keywords: Fault; Fault core; Particle size distribution; Power law; Scaling

1. Introduction

Cataclastic fault zones include a relatively narrow fault core where fault rocks occur (e.g. Aydin, 1978; Chester et al., 1993; Evans et al., 1997). Fault cores may contain slip surfaces or may be bounded by them on one or both sides. Fracture-bearing damage zones typically flank the fault core on one or both sides, and are bounded by the protolith (e.g. Caine et al., 1996; Flodin and Aydin, 2004; Kim et al., 2004).

Data on the particle size distribution of fault rocks and on their scaling laws are primary to infer and predict the hydraulic (e.g. Bear, 1972; Shepherd, 1989; Antonellini and Aydin, 1994; Main et al., 2000; Wibberley and Shimamoto, 2003; Agosta et al., 2006; Micarelli et al., 2006; Wilson et al., 2006) and frictional (e.g. Morgan and Boettcher, 1999; Mair et al., 2002; Wilson et al., 2005) properties of cataclastic fault zones. The particle size distribution of fault rocks usually follows power laws with the three-dimensional fractal dimension (D) ranging in nature between $\sim$1.9 and $\sim$5.5 (e.g. Blenkinsop, 1991; Storti et al., 2003). Despite the large number of published data on the particle size distributions of fault rocks, most data cover a limited range of particle sizes, particularly for natural fault rocks. So far, two principal approaches have been taken to determine the size distributions of fault rocks. A first method consists in measuring the size of particles on rock thin sections at different magnifications (e.g. Blenkinsop, 1991), whereas a second one involves a sieving procedure (e.g. Hooke and Iverson, 1995).

* Tel.: +39 06 5488 8016; fax: +39 06 5488 8201.
E-mail address: billi@uniroma3.it

0191-8141/$ - see front matter © 2007 Elsevier Ltd. All rights reserved.
doi:10.1016/j.jsg.2007.06.007

The first method is appropriate for indurated fault rocks, whereas the second one applies well to loose or poorly indurated fault rocks. Because optical and scanning electron microscopes can highly magnify thin sections, the particle size distributions determined through these devices are usually well documented for what concerns the small particles. On the contrary, the size of coarse particles (i.e. $> \sim 1$ mm) cannot be properly documented under the microscope because of the limited surface of thin sections, and the limited angle of view of microscopes.

The sieving procedure can be suitably applied to particle populations with size even greater than 1 cm, but, because of the adhesive effects among the small particles, this technique may provide biased data for particle sizes lower than approximately 0.07 mm (Krumbein and Pettijohn, 1990). Moreover, the sieving technique provides suitable results for near-rounded shapes of grains; otherwise, image analysis is more accurate (Rawling and Goodwin, 2003).

In addition to the above-mentioned, classical methods of particle size analysis, in the last years, laser particle size analysers have been produced. By measuring the size of particles using the diffraction and diffusion of a laser beam, these devices have provided suitable size distribution curves in the 0.05–1000 μm range for fault rock particles (Crawford, 1998; Flodin et al., 2005) and will probably become soon the standard instruments for particle size analyses of loose rocks and sediments.

In loose carbonate fault rocks, the distribution of particle sizes has been studied in the 0.125–4.0 mm range by a sieving method (Storti et al., 2003; Billi et al., 2003; Billi and Storti, 2004). Recently, the upper bound of the analysed size range has been extended to approximately 16 mm (Agosta and Aydin, 2006). Results show that the particle size distributions of carbonate fault rocks follow power laws with D-values ranging between $\sim$2.00 and $\sim$3.50; however, the limitation of the studied range of sizes (i.e. particularly toward the small particles) spawns doubt about the extent of the power law scaling, which, at least when $D > 3$, must have a lower bound. A full particle size distribution with $D > 3$ would, in fact, mean that particles reciprocally interpenetrated (Steacy and Sammis, 1992; Heilbronner and Keulen, 2006).

The aim of this study is to analyze the particle size distribution of natural carbonate fault rocks and to determine the size range and both type and extent of their scaling laws. To do so, samples of granular, carbonate, fault rocks have been collected from various sites in central Italy (Fig. 1 and Table 1). Their particle size distribution has been determined by combining sieving and sedimentation methods (Krumbein and Pettijohn, 1990). The combination of these two methods has led to the characterization of the particle size distributions across a broad range of sizes. These data may result useful as input numbers in numerical models addressing, for instance, the frictional and hydraulic behaviours of granular fault cores (e.g. Morgan, 1999; Hecht, 2000; O'Brien et al., 2003) across

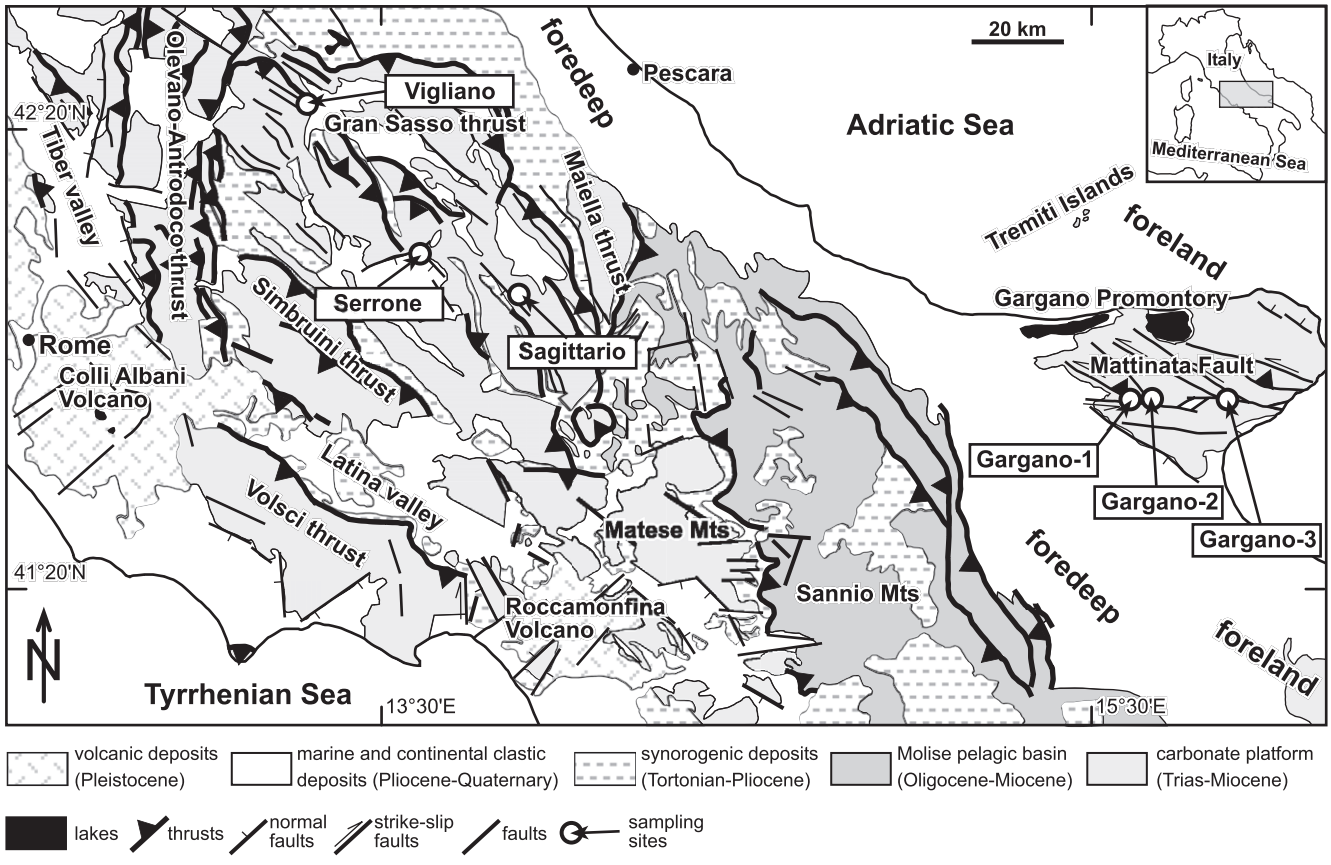

Fig. 1. Geological map of the central Italy (modified from Bigi et al., 1992) with locations for the studied fault cores. See Table 1 for coordinates of fault locations.

Table 1
Data about the study sites, fault cores, and samples

Fault/site	Long. East	Lat. North	Sample	Sample weight (g)	Density (g/cm^3)	Protolith type (age)	Tectonic environment	Fault kinematics	Fault azimuth	Fault dip	Slick. pitch
Gargano-1	15°36′	41°45′	2GB01	1991	2.68	Pl. limestone (Jurassic)	Foreland	Reverse	N157°	31°SWward	87°
Gargano-1	15°36′	41°45′	2GB02	3666	2.67	Pl. limestone (Jurassic)	Foreland	Reverse	N157°	31°SWward	87°
Vigliano	13°16′	42°24′	2GB03	1187	2.71	Pl. limestone (Cretaceous)	Thrust belt	Reverse	N110°	17°Sward	61°
Vigliano	13°16′	42°24′	2GB04	1400	2.72	Pl. limestone (Cretaceous)	Thrust belt	Reverse	N110°	17°Sward	61°
Gargano-2	15°41′	41°45′	2GB05	2421	2.67	Pl. limestone (Jurassic)	Foreland	Transpressive	N124°	71°Nward	37°
Gargano-2	15°41′	41°45′	2GB06	921	2.67	Pl. limestone (Jurassic)	Foreland	Transpressive	N124°	71°Nward	37°
Gargano-3	15°55′	41°45′	2GB07	1149	2.66	Pl. limestone (Jurassic)	Foreland	Strike-slip	N092°	88°Sward	3°
Gargano-3	15°55′	41°45′	2GB08	2561	2.66	Pl. limestone (Jurassic)	Foreland	Strike-slip	N092°	88°Sward	3°
Sagittario	13°56′	41°58′	2GB09	1650	2.72	Pl. limestone (Jurassic)	Thrust belt	Extensional	N137°	54°SWward	86°
Sagittario	13°56′	41°58′	2GB10	1844	2.71	Pl. limestone (Jurassic)	Thrust belt	Extensional	N137°	54°SWward	86°
Serrone	13°37′	42°04′	2GB11	6501	2.67	Pl. limestone(Cretaceous)	Thrust belt	Extensional	N137°	62°SWward	92°
Serrone	13°37′	42°04′	2GB12	1819	2.67	Pl. limestone,(Cretaceous)	Thrust belt	Extensional	N137°	62°SWward	92°

"Long." is longitude, "lat." is latitude, "pl." is platform, and "slick." is slickenside lineation.

carbonate strata. Fault cores in carbonate strata are, in fact, known both as potential hydraulic barriers in hydrocarbon and water reservoirs (e.g. Mancini et al., 2004; Celico et al., 2006) and as potential foci for seismic faulting (e.g. Miller et al., 2004). Agosta et al. (2006) and Micarelli et al. (2006), for instance, have recently measured permeabilities between 10^{-16} and 10^{-20} m^2 and on the order of 10^{-16} m^2, respectively, within granular carbonate fault cores. These data prove that fault cores in carbonate rocks can act as hydraulic barriers.

2. Methods

Twelve samples of loose-to-poorly indurated, carbonate fault rocks (i.e. fault gouge and breccia) were collected from six granular fault cores (i.e. two adjacent samples from each fault core; the adjacent samples are henceforth named sample pairs; e.g. Figs. 2a,b). In this paper, the terms fault breccia and fault gouge are used to indicate the relative average size of the sample particles within each sample pair, i.e. a fault breccia sample contains particles that are averagely coarser than the particles forming the adjacent sample of fault gouge.

The analysed fault cores are exposed in the Appennines foreland fold-thrust belt, central Italy (Fig. 1). Within the framework of convergence between the African and Eurasian plates, the Apennines belt grew during Paleogene-Neogene times as an east-verging orogenic wedge overriding the Adriatic-Apulian foreland (Malinverno and Ryan, 1986). The selected sites (Table 1) are characterized by similar protolith (i.e. Mesozoic platform carbonate strata) and by different fault attitude, kinematics, tectonic environment, and, possibly, displacement. Fault displacement, in particular, could not be assessed because of the absence of stratigraphic horizons suitable for displacement measurements.

Sample pairs 2GB01–2GB02, 2GB05–2GB06, and 2GB07–2GB08 come from three sites along the regional strike-slip Mattinata Fault (Salvini et al., 1999; Brankman and Aydin, 2004) in the Gargano foreland area, where outcrop-scale strike-slip transcontractional and reverse fault cores are exposed (Figs. 2a,b). The sample pair 2GB03–2GB04 comes from a reverse fault core, whereas the two sample pairs 2GB09–2GB10 and 2GB11–2GB12 come from extensional fault cores (Figs. 2c,d). The latter three sample pairs (2GB01–2GB02, 2GB05–2GB06, and 2GB07–2GB08) were collected from sites in the Apennines thrust-fold belt (Vittori et al., 1991; Agosta and Aydin, 2006) (Table 2).

Sampling was done by removing rocks from the exposure by means of non-destructive instruments and actions. Non-destructive penetration of rocks was possible for their substantial non-cohesive status (Fig. 3). To avoid biased results induced by the effect of surface weathering, before sampling, a 20–30 cm thick layer of surface cataclastic material was removed from the exposures.

The particle size distribution of samples was determined by a sieving method for the material larger than 0.063 mm in size, and by a sedimentation method (i.e. within a pipette) for the material passing through the sieve with a mesh size of

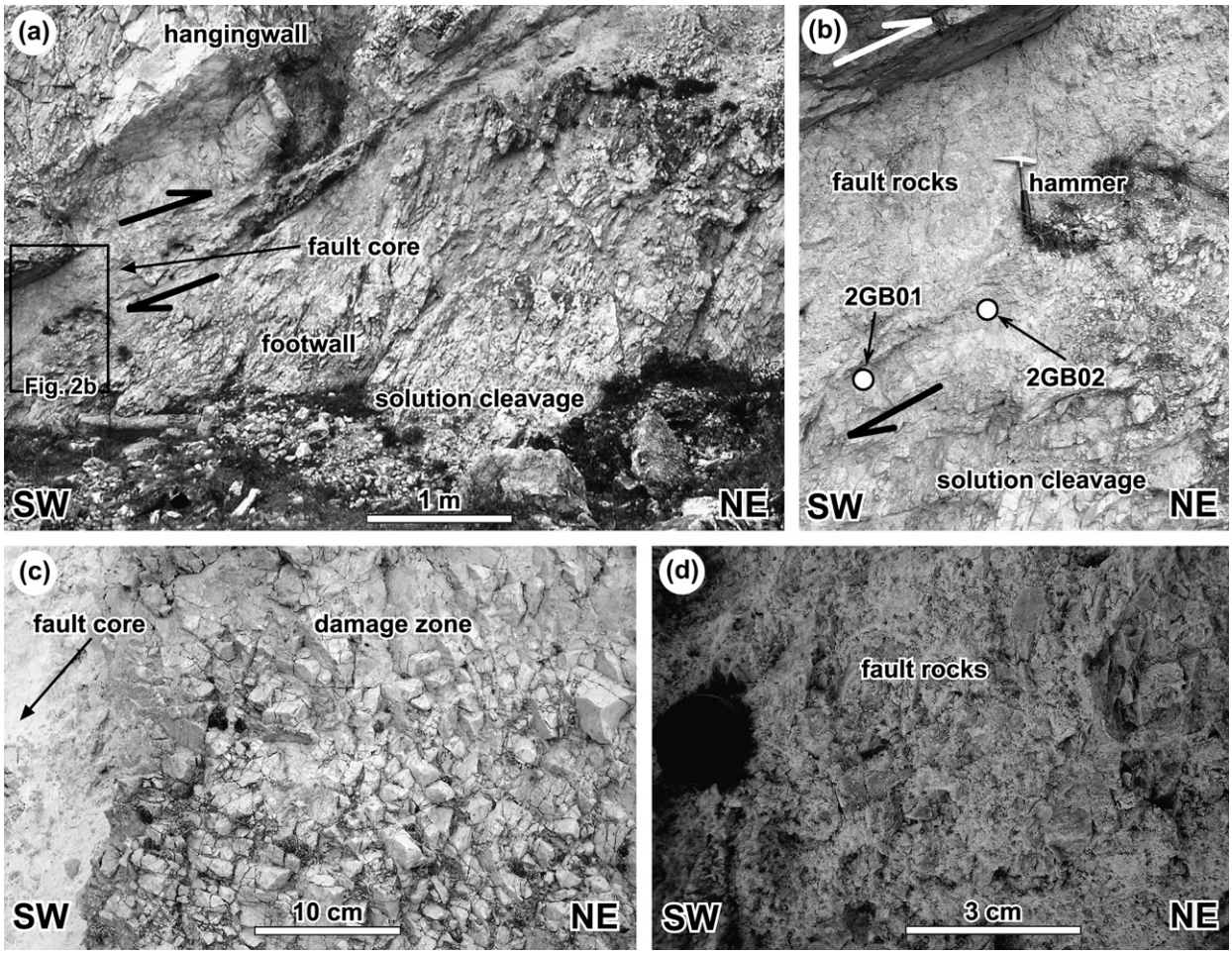

Fig. 2. Photographs of some studied fault cores. (**a**) Gargano-1 site exposure (i.e. reverse fault). On the hangingwall, a well developed set of SW-dipping solution cleavage surfaces occurs as compatible with the fault reverse kinematics. The solution domains are intensely fragmented. (**b**) Enlargement from (a). Note the cataclastic fabric of fault rocks, in which any pre-existing tectonic (e.g. solution surfaces) or sedimentary (e.g. strata) structure is entirely obliterated. No solution structures (e.g. stylolites) occur within the fault core. (**c**) Serrone site (i.e. extensional fault). The damage zone near the fault core is intensely fractured. The pristine carbonate rock is transformed into an assemblage of near-cubic polyhedron a few centimetres in size. (**d**) Fault core at the Serrone site (low *D*-values). Note the cataclastic fabric consisting of several, coarse, angular particles, which are in contact with one another. No solution structures (e.g. stylolites) occur within the fault core.

0.063 mm (Krumbein and Pettijohn, 1990). In synthesis, the sieving method consisted in: (1) disaggregating the sample in water by an ultrasonic device; (2) drying the disaggregated sample at 105 °C; (3) dry-weighting the sample; (4) sieving the sample through a series of sieves; the smallest sieve had a mesh size of 0.063 mm; and (5) weighting the residue in each sieve.

To do the sedimentation analysis, the material passing through the sieve with a mesh size of 0.063 mm was dispersed in water with a deflocculating agent. The entire procedure adopted in this work to accomplish particle size analysis by the sedimentation method is described in detail in Poppe et al. (2000). In summary, the sedimentation method relies upon the settling velocity differentiation by sampling at certain depths in the settling cylinder at certain time intervals, using the obtained settling velocities to divide the sample into size fractions. The lowest size considered in this analysis is 0.0005 mm. Under this size, the sedimentation method may provide unsuitable results (Krumbein and Pettijohn, 1990).

Weight data from the sieving and sedimentation analyses (i.e. for each size class) were transformed into weight-equivalent numbers of spherical particles. Such data processing relies upon the assumption verified in several previous papers of the nearly spherical shape of fault rock particles (Hooke and Iverson, 1995; Billi et al., 2003; Storti et al., 2003, 2006; Chambon et al., 2006; Heilbronner and Keulen, 2006). The number of weight-equivalent spherical particles was obtained by dividing the weight of each size fraction by the weight of a sphere having the density of the sample as measured in a water pycnometer and the size pertaining to the considered fraction (Table 2). To visualize the particle size distributions and to determine the scaling laws, the numbers of weight-equivalent spherical particles were plotted in log-log diagrams versus the corresponding size classes. These data were fit with the following power law regression:

Table 2
Numbers of weight-equivalent spherical particles sorted by size classes

2GB01		2GB02		2GB03		2GB04		2GB05		2GB06	
d	*N*	*d*	*N*	*d*	*N*	*d*	*N*	*d*	*N*	*d*	*N*
4	1	4	3	8	2	8	2	16	1	16	1
2	851	2	4453	4	496	4	536	8	431	8	251
1	10534	1	54551	2	14172	2	11865	4	3590	4	899
0.5	148421	0.5	813081	1	80179	1	120513	2	35666	2	13033
0.25	504707	0.25	8343845	0.5	753716	0.5	859626	1	239448	1	71069
0.125	9577542	0.125	52467968	0.25	3654209	0.25	3803539	0.5	2298595	0.5	780629
0.063	86002716	0.063	471142526	0.125	11554522	0.125	97395707	0.25	6556308	0.25	2010898
0.032	868996136	0.032	4760565263	0.063	235629408	0.063	315090827	0.125	60387096	0.125	17478115
0.016	22959111111	0.016	22544063158	0.032	1917144180	0.032	3207056622	0.063	152263672	0.063	112130568
0.008	1.54436E + 11	0.008	2.24341E + 11	0.016	2.2033E + 10	0.016	11077549140	0.032	931700000	0.032	805247811
0.004	9.27584E + 11	0.004	1.14878E + 12	0.008	9.3286E + 10	0.008	78172416000	0.016	5.493E + 09	0.016	4388369400
0.002	1.91452E + 13	0.002	6.42014E + 13	0.004	8.3077E + 11	0.004	2.90617E + 11	0.008	4.225E + 10	0.008	3.2409E + 10
0.001	1.92341E + 14	0.001	7.38371E + 14	0.002	5.6977E + 12	0.002	2.56322E + 12	0.004	9.693E + 11	0.004	2.5041E + 11
0.0005	5.88211E + 15	0.0005	3.26035E + 15	0.001	7.0817E + 13	0.001	3.10636E + 13	0.002	7.908E + 12	0.002	7.3641E + 11
				0.0005	1.7826E + 14	0.0005	3.09651E + 14	0.001	3.448E + 13	0.001	5.112E + 12
								0.0005	6.615E + 11	0.0005	1.2567E + 12
2GB07		2GB08		2GB09		2GB10		2GB11		2GB12	
d	*N*	*d*	*N*	*d*	*N*	*d*	*N*	*d*	*N*	*d*	*N*
16	3	16	1	16	1	16	2	32	2	32	1
8	351	8	689	8	534	8	566	16	582	16	129
4	2090	4	5906	4	3713	4	4229	8	2052	8	556
2	24102	2	27628	2	21637	2	20626	4	10146	4	2793
1	89037	1	234317	1	160677	1	106360	2	26554	2	16609
0.5	420475	0.5	1619051	0.5	738529	0.5	724488	1	137470	1	81153
0.25	3522425	0.25	6272128	0.25	2530028	0.25	6884975	0.5	694160	0.5	379613
0.125	17218516	0.125	68132636	0.125	35589840	0.125	53424122	0.25	3260753	0.25	901073
0.063	146869476	0.063	275931621	0.063	109440760	0.063	297665636	0.125	8231293	0.125	3546275
0.032	1123668780	0.032	1482055830	0.032	1126254800	0.032	1406482110	0.063	34521407	0.063	17919293
0.016	3471214500	0.016	12237212100	0.016	5500038500	0.016	6660046620	0.032	122849099	0.032	96085544
0.008	1.9508E + 10	0.008	62100041400	0.008	2.7561E + 10	0.008	31061853720	0.016	383327864	0.016	349336210
0.004	6.2573E + 10	0.004	3.34375E + 11	0.004	2.4229E + 11	0.004	1.35447E + 11	0.008	2301482491	0.008	1324448015
0.002	6.1571E + 11	0.002	1.41175E + 12	0.002	1.1103E + 12	0.002	6.02979E + 11	0.004	5142492690	0.004	3402121018
0.001	1.0463E + 11	0.001	1.68363E + 12	0.001	2.0188E + 11	0.001	2.13072E + 12	0.002	3721592680	0.002	2237448015
0.0005	9.0191E + 10	0.0005	1.00478E + 12	0.0005	2.7711E + 11	0.0005	2.00423E + 12	0.001	7824192900	0.001	3278478005
								0.0005	1.1795E + 10	0.0005	3320001245

"*d*" is particle diameter in mm and "*N*" is number of weight-equivalent spherical particles.

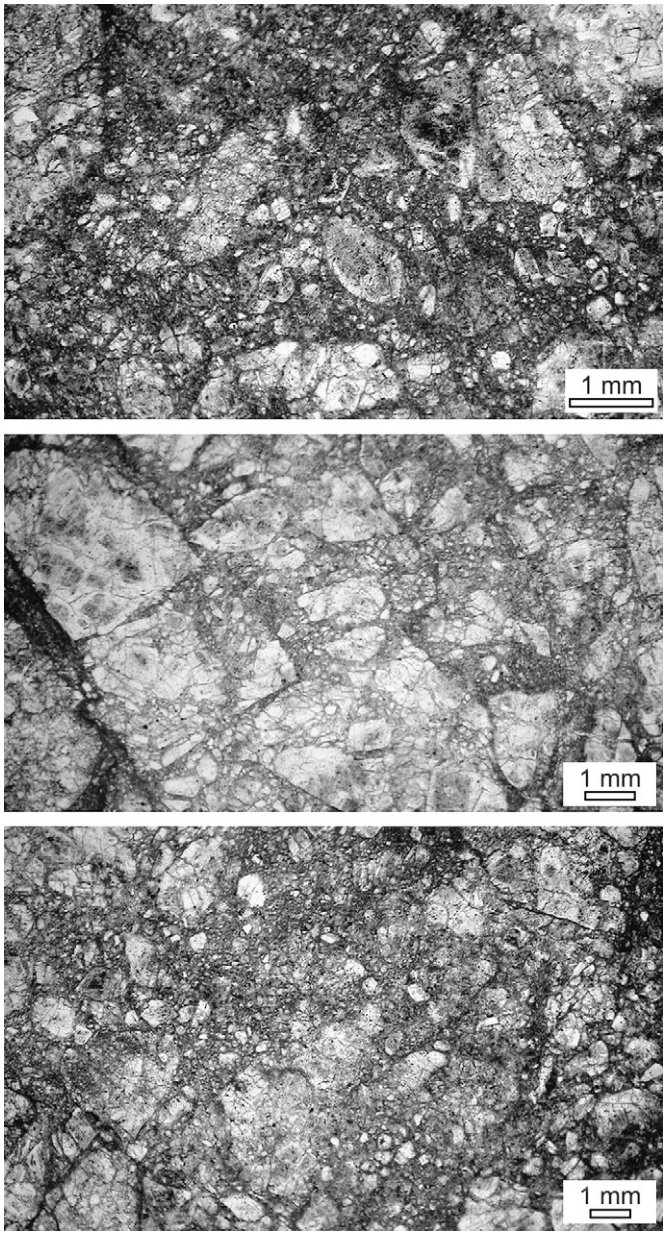

Fig. 3. Microscope photographs showing the disaggregated to poorly-aggregated fabric of the fault core rocks. Thin-sections were obtained from rare, poorly-cohesive, samples of the studied fault cores, which are generally non-cohesive. For this reason, these photographs may be poorly representative of the analysed, non-cohesive rocks.

$$\log N = -D \log d + A \quad (1)$$

where d is the particle size class (i.e. the diameter of the spherical particles), N is the number of equivalent spherical particles, and A is a sample-specific constant. The power law best-fit was established by running the appropriate best-fitting procedure (i.e. Eq. (1)) using the GRAPHER 2 software produced by Golden Software Inc. Eq. (1) is linear in a log-log space and D is the slope of the best-fit line. In the case of power law distributions, D indicates the proportion of particles of different sizes in one sample, i.e. the higher the value of D, the larger the proportion of small particles (Blenkinsop, 1991). D is commonly identified as the "fractal dimension". We henceforth use this term; however, in this work, such a term does not imply that the size distributions of the studied fault rock particles are fractal over the entire size range nor it means that the process of particle fragmentation was fractal (Storti et al., 2003; Heilbronner and Keulen, 2006). Alternatively, D is indicated as "mass dimension" (Sammis and King, 2007).

3. Results

Numbers of weight-equivalent spherical particles (Table 2) plotted versus size classes in log-log diagrams follow linear trends across most of the size ranges (Fig. 4 and Table 3). In the size interval in which the linear trends of data occur, Eq. (1) well fits the particle size data. D-values are between ~2.0 and ~3.5 and the related coefficients of determination (R^2) are between 0.994 and 0.999 (Table 3).

In each sample pair, the particle size distributions for the two samples are characterized by strong similarities consisting in (Tables 3 and 4): (1) the extent of the particle size ranges; (2) the extent of the power law scaling; and (3) the values of D. These same parameters, in contrast, differ among samples from different sample pairs (i.e. different fault cores).

For low D-values ($D \approx 2.0$), the upper bound for the particle size range falls between 32 mm and 64 mm, whereas the lower bound is less than 0.0005 mm. The upper bound for the power law scaling falls between 16 mm and 32 mm, whereas the lower bound falls between 0.002 mm and 0.004 mm.

For high D-values ($D \approx 3.2$–3.5), the upper bound for the particle size range falls between 2 mm and 4 mm, whereas the lower bound is less than 0.0005 mm. The upper bound for the power law scaling falls between 4 mm and 8 mm, whereas the lower bound is probably less than 0.0005 mm.

For intermediate D-values ($D \approx 2.7$), the upper bound for the particle size range falls between 16 mm and 32 mm, whereas the lower bound is less than 0.0005 mm. The upper bound for the power law scaling falls between 8 mm and 16 mm, whereas the lower bound falls between 0.001 mm and 0.0005 mm.

The above observations concerning the lower bounds for the power law intervals are synthesized in Fig. 5, which shows inverse correlation between D-values and the lower bounds for the power law intervals.

4. Discussion

The most important result arising from the analysis of the fault rock samples studied in this paper is that the size distributions of fault rock particles follow power law trends over approximately four orders of magnitude, with no evidence of gaps or scaling changes (Fig. 4 and Table 4). This scaling law applies well to all studied fault rocks regardless of the tectonic environment and the fault geometry, kinematics, and, possibly, displacement. An increase of D corresponds with a reduction of the maximum size of particles, and with a tendency of the power law interval to include progressively smaller particles (Fig. 5 and Table 4); however, the reduction of the maximum size of particles with increasing D-values

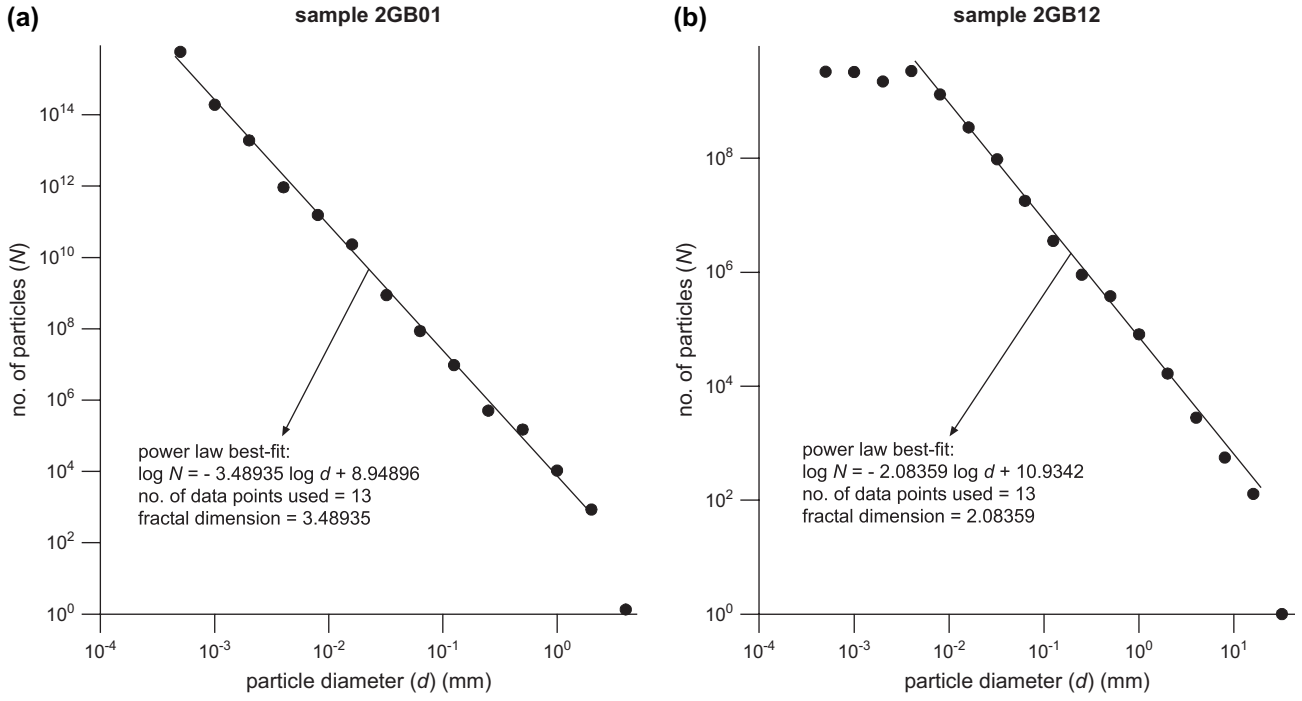

Fig. 4. Log-log diagrams showing the relationship between the size (d) of particles (i.e. the diameter of weight-equivalent spherical particles) and the number (N) of particles for samples 2GB01 (**a**) and 2GB12 (**b**). Data are listed in Table 2.

may not be a reliable indicator of the fault rock evolution. The recorded maximum size of particles may, in fact, be affected by a censoring bias connected with the sample size (i.e. total weight). In other words, large particles may be absent in some samples because the samples are too small to include the entire population of particle size, particularly, the largest ones.

It is known from previous studies on the analysed fault cores and on other fault cores in carbonate rocks, that the deformation mechanisms leading to the observed particle comminution are mostly fragmentation and abrasive wear (Storti et al., 2003; Billi, 2005; Micarelli et al., 2006). The lack of evidence for stylolites and other dissolution-related structures within the matrix of the studied fault cores suggests that carbonate dissolution and more in general hydrous alteration during cataclasis was possibly minimized (e.g. Goodwin and Wenk, 1995).

Four major inferences deriving from the results presented in this paper are worthy of discussion:

(1) The extension toward the small particles of the power law interval with increasing D-values suggests that, whereas for particle size distributions with $D \approx 2.0$ the particles ≈ 0.002 mm in size are fragments not undergoing substantial comminution (i.e. spectator fragments according to Mair et al., 2002), for D approaching 2.5, these same particles start to be actively comminuted. In other words, in particle populations with low D-values, small particles are volumetrically rarer and hence poorly comminuted because stresses are concentrated at the contact points between large particles (Fig. 6). When large particles become volumetrically rarer, stresses start to be transmitted also through the small particles that become volumetrically less rare. The same evolution observed for the particles ≈ 0.002 mm in size applies also to the

Table 3
Best-fit equations and related statistical parameters

Sample	Fractal dimension	No. of data points	No. of data points used	Coefficient of determination (R^2)	Power law best-fit equation (Eq. (1))
2GB01	3.48935	14	13	0.997612	$\log N = -3.48935 \log d + 8.94896$
2GB02	3.25799	14	13	0.996269	$\log N = -3.25799 \log d + 10.9352$
2GB03	2.95046	15	14	0.996845	$\log N = -2.95046 \log d + 11.0632$
2GB04	2.85714	15	14	0.995290	$\log N = -2.85714 \log d + 11.3839$
2GB05	2.72528	16	14	0.994806	$\log N = -2.72528 \log d + 12.0061$
2GB06	2.67154	16	14	0.998267	$\log N = -2.67154 \log d + 11.1198$
2GB07	2.54251	16	13	0.997630	$\log N = -2.54251 \log d + 11.4306$
2GB08	2.59745	16	13	0.998890	$\log N = -2.59745 \log d + 12.2348$
2GB09	2.58359	16	13	0.998727	$\log N = -2.58359 \log d + 11.7206$
2GB10	2.54698	16	13	0.997000	$\log N = -2.54698 \log d + 11.9085$
2GB11	1.96186	17	13	0.998299	$\log N = -1.96186 \log d + 11.8553$
2GB12	2.08359	17	13	0.997440	$\log N = -2.08359 \log d + 10.9342$

Table 4
Extent of size range and power law scaling for particles from fault core samples

Fault	Sample	Fractal dimension (D)	Size range extent (mm)		P. law extent (mm)
			U. bound	L. bound	L. bound
Gargano-1	2GB01	3.48935	8 < > 4	<0.0005	<0.0005
Gargano-1	2GB02	3.25799	8 < > 4	<0.0005	<0.0005
Vigliano	2GB03	2.95046	16 < > 8	<0.0005	<0.0005
Vigliano	2GB04	2.85714	16 < > 8	<0.0005	<0.0005
Gargano-2	2GB05	2.72528	32 < > 16	<0.0005	0.001 < > 0.0005
Gargano-2	2GB06	2.67154	32 < > 16	<0.0005	0.001 < > 0.0005
Gargano-3	2GB07	2.54251	32 < > 16	<0.0005	0.002 < > 0.001
Gargano-3	2GB08	2.59745	32 < > 16	<0.0005	0.002 < > 0.001
Sagittario	2GB09	2.58359	32 < > 16	<0.0005	0.002 < > 0.001
Sagittario	2GB10	2.54698	32 < > 16	<0.0005	0.002 < > 0.001
Mt Serrone	2GB11	1.96186	64 < > 32	<0.0005	0.004 < > 0.002
Mt Serrone	2GB12	2.08359	64 < > 32	<0.0005	0.004 < > 0.002

"U." is upper, "l." is lower, "p." is power, and "< >" is between.

particles ≈0.0005 mm in size. These particles enter the power law interval for particle size distributions with $D \approx 3.2$. This inference suggests that the lower boundary to the power law may extend toward the particles possibly even smaller than 0.0005 mm (e.g. Chester et al., 2005) as a function of the comminution progression (Sammis and King, 2007). In the future, further analyses with appropriate instruments (e.g. progressively higher definition scanning electron microscopes) may clarify this point and investigate the grinding limit (Kendall, 1978) of fault rock particles that should be, for instance, approximately 1–2 μm in quartziferous particles (Prasher, 1987).

(2) It is known that the friction of granular fault rocks is low when coarse particles are embedded in a matrix of small particles. The presence of gouge tends to suppress unstable sliding (i.e. sudden changes in friction coefficient with sliding velocity, Brace and Byerlee, 1966) in most laboratory faults (Marone et al., 1992; Lockner and Byerlee, 1993; Beeler et al., 1996) and numerical simulations (Morgan, 1999). As shown by Sammis et al. (1987), in a particle population with $D \geq 2.58$, coarse particles are well cushioned within a fine matrix. In this paper, the disappearance of the coarse particles in moving from particle size distributions with $D \approx 2.5$–2.6 to distributions with $D \approx 3.2$–3.5 suggests that, even in fault rocks with $D \geq 2.58$, the coarse particles might have been brought frequently into contact to form bridges where the stress concentrated and led to the particle bulk crushing (Mandl et al., 1977; Hooke and Iverson, 1995; Sammis and King, 2007; see also the mechanism of selective fracture of larger particles in Blenkinsop, 1991). The formation of such strong bridges increases the fault friction until the particles forming the bridge are crushed. If repeated, this process may generate a stick-slip fault behaviour (Brace and Byerlee, 1966; Byerlee et al., 1978). The above inference is valid upon the reasonable assumption of a direct relationship between comminution of fault rocks (i.e. increasing D-values; e.g. Marone and Scholz, 1989; Blenkinsop, 1991) and fault displacement (Engelder, 1974; Mandl et al., 1977; House and Gray, 1982; Hooke and Iverson, 1995; Sammis and King, 2007). Moreover, as stated above, this inference may be invalid in the case the abundance of large particles in the analysed samples is biased by the limited size of samples.

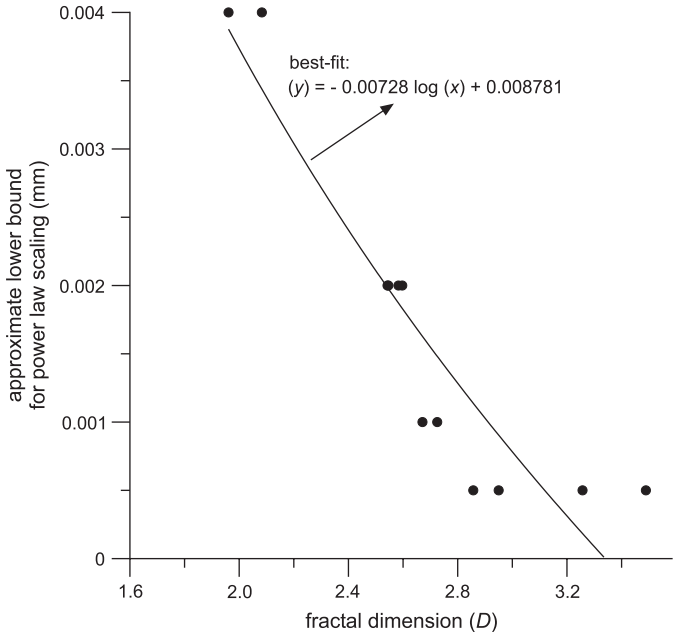

Fig. 5. Diagram for fractal dimension versus the lower bound for the power law intervals of fault core particles. The diagram shows inverse correlation of data.

(3) The porosity of granular fault rocks mostly depends on the particle sizes and packing (Antonellini and Aydin, 1995). Theoretically, the porosity of a fractal mix diminishes to zero for D approaching the theoretical upper limit of 3 (Steacy and Sammis, 1992; Hecht, 2000). However, particle size data from this paper and from previous ones (Blenkinsop, 1991; Storti et al., 2003) show that D in nature exceeds 3 because the power law fits only a limited size interval (Steacy and Sammis, 1992; Heilbronner and Keulen, 2006). Hence, to correctly simulate the porosity of fault rocks, it is necessary

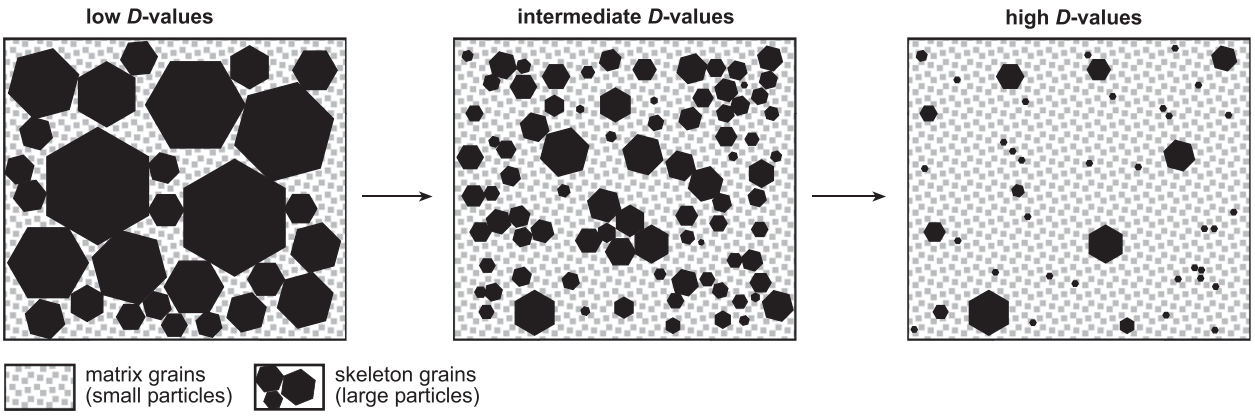

Fig. 6. Schematic diagram showing the evolution of the fault rock particle population with increasing *D*-values. The fractional volume of smaller particles (matrix) increases as *D* increases (e.g. Blenkinsop, 1991). It follows that small particles become a more significant constituent of the fault rock and therefore will be more easily involved in further comminution, thereby increasing *D* further through positive feedback. Stresses leading to particle comminution concentrate at the contact points between large particles for low *D*-values, whereas, for high *D*-values, the large particles are embedded in a fine matrix and stresses are therefore mostly transmitted through the matrix, in which the small particles undergo brittle comminution.

to know the particle scaling law and the relative extent. The data supplied in this paper provide efficient means, at least in carbonate rocks, to model the packing configurations of fault rock particles and to compute the related porosity (e.g. Hecht, 2004).

5. Conclusions

The combination of sieving and sedimentation methods for the analysis of carbonate fault rocks provided particle numbers by size classes across a wide range of sizes. These data conform to power law trends across approximately four orders of magnitude or even more. The reproducibility of the analyses is demonstrated by the similitude of results from independent analyses on adjacent samples collected in the same fault cores. Although further analyses are necessary to generalize the results and to investigate the size distribution of particles smaller than 0.0005 mm and the grinding limit of these particles, the recognition and definition of power law scaling rules for fault rock particles allow, at least for carbonate fault rocks, fractal based interpolations, which are a powerful predictive means for a wide variety of problems in geology and geophysics, such as those concerning hydrocarbon reservoirs, aquifers, waste repositories, mineralizations, and seismic faults.

Acknowledgments

F. Salvini and F. Storti are thanked for their perceptive supervision during previous studies on fault rocks. F. Agosta, G. Di Toro, E. Flodin, L. Gomez, and T. Manzocchi provided insightful comments on the last or early versions of the manuscript.

References

Agosta, F., Aydin, A., 2006. Architecture and deformation mechanism of a basin-bounding normal fault in Mesozoic platform carbonates, central Italy. Journal of Structural Geology 28, 1445–1467.

Agosta, F., Prasad, M., Aydin, A., 2006. Physical properties of carbonate fault rocks, Fucino basin, central Italy: implications for fault seal in platform carbonates. Geofluids 6, 1–14.

Antonellini, M., Aydin, A., 1994. Effect of faulting on fluid flow in porous sandstones: petrophysical properties. American Association of Petroleum Geologists Bulletin 78, 355–377.

Antonellini, M., Aydin, A., 1995. Effect of faulting on fluid flow in porous sandstones: geometry and spatial distribution. American Association of Petroleum Geologists Bulletin 79, 642–671.

Aydin, A., 1978. Small faults formed as deformation bands in sandstone. Pure and Applied Geophysics 116, 913–930.

Bear, J., 1972. Dynamics of Fluids in Porous Media. Dover Publications, New York, 764 pp.

Beeler, N.M., Tullis, T.E., Blanpied, M.L., Weeks, J.D., 1996. Frictional behavior of large displacement experimental faults. Journal of Geophysical Research 101, 8697–8715.

Bigi, G., Cosentino, D., Parotto, M., Sartori, R., Scandone, P. (Eds.), 1992, Structural Model of Italy, scale, 1. SELCA, Florence, p. 500,000.

Billi, A., 2005. Grain size distribution and thickness of breccia and gouge zones from thin (<1 m) strike-slip fault cores in limestone. Journal of Structural Geology 27, 1823–1837.

Billi, A., Storti, F., 2004. Fractal distribution of particle size in carbonate cataclastic rocks from the core of a regional strike-slip fault zone. Tectonophysics 384, 115–128.

Billi, A., Salvini, F., Storti, F., 2003. The damage zone-fault core transition in carbonate rocks: implications for fault growth, structure and permeability. Journal of Structural Geology 25, 1779–1794.

Blenkinsop, T.G., 1991. Cataclasis and processes of particle size reduction. Pure and Applied Geophysics 136, 59–86.

Brace, W.F., Byerlee, J.D., 1966. Stick slip as a mechanism for earthquakes. Science 153, 990–992.

Brankman, C., Aydin, A., 2004. Uplift and contractional deformation along a segmented strike-slip fault system: the Gargano Promontory, southern Italy. Journal of Structural Geology 26, 807–824.

Byerlee, J., Mjachkin, V., Summers, R., Voevoda, O., 1978. Structures developed in fault gouge during stable sliding and stick-slip. Tectonophysics 44, 161–171.

Caine, J.S., Evans, J.P., Forster, C.B., 1996. Fault zone architecture and permeability structure. Geology 24, 1025–1028.

Celico, F., Petrella, E., Celico, P., 2006. Hydrogeological behaviour of some fault zones in a carbonate aquifer of Southern Italy: an experimentally based model. Terra Nova 18, 308–313.

Chambon, G., Schmittbuhl, J., Corfdir, A., 2006. Frictional response of a thick gouge sample: 1. Mechanical measurements and microstructures. Journal of Geophysical Research 111, B09308, doi:10.1029/2004JB003339.

Chester, F.M., Evans, J.P., Biegel, R.L., 1993. Internal structure and weakening mechanisms of the San Andreas Fault. Journal of Geophysical Research 98, 771–786.

Chester, J.S., Chester, F.M., Kronenberg, A.K., 2005. Fracture surface energy of the Punchbowl fault, San Andreas system. Nature 437, 133–136.

Crawford, B.R., 1998. Experimental fault sealing: shear band permeability dependency on cataclastic fault gouge characteristics. In: Coward, M.P., Daltaban, T.S., Johnson, H. (Eds.), Structural Geology in Reservoir Characterization, 127. Geological Society of London Special Publications, pp. 27–47.

Engelder, T., 1974. Cataclasis and the generation of fault gouge. Geological Society of America Bulletin 85, 1515–1522.

Evans, J.P., Forster, C.B., Goddard, J.V., 1997. Permeability of fault-related rocks, and implications for hydraulic structure of fault zones. Journal of Structural Geology 19, 1393–1404.

Flodin, E., Aydin, A., 2004. Faults with asymmetric damage zones in sandstone, Valley of Fire State Park, southern Nevada. Journal of Structural Geology 26, 983–988.

Flodin, E.A., Gerdes, M., Aydin, A., Wiggins, W.D., 2005. Petrophysical properties and sealing capacity of fault rock, Aztec Sandstone, Nevada. In: Sorkhabi, R., Tsuji, Y. (Eds.), Faults, Fluid Flow, and Petroleum Traps, 85. AAPG Memoir, pp. 197–217.

Goodwin, L.B., Wenk, H.R., 1995. Development of phyllonite from granodiorite: mechanisms of grain-size reduction in the Santa Rosa mylonite zone, California. Journal of Structural Geology 17, 689–707.

Hecht, C.A., 2000. Appolonian packing and fractal shape of grains improving geomechanical properties in engineering geology. Pure and Applied Geophysics 157, 487–504.

Hecht, C.A., 2004. Geomechanical models for clastic grain packing. Pure and Applied Geophysics 161, 331–349.

Heilbronner, R., Keulen, N., 2006. Grain size and grain shape analysis of fault rocks. Tectonophysics 427, 199–216.

Hooke, R.LeB., Iverson, N.R., 1995. Grain-size distribution in deforming subglacial tills: role of grain fracture. Geology 23, 57–60.

House, W.M., Gray, D.R., 1982. Cataclasites along the Saltville thrust, U.S.A., and their implications for thrust-sheet emplacement. Journal of Structural Geology 4, 257–269.

Kendall, K., 1978. The impossibility of comminuting small particles by compression. Nature 272, 710–711.

Kim, Y.-S., Peacock, D.C.P., Sanderson, D.J., 2004. Fault damage zones. Journal of Structural Geology 26, 503–517.

Krumbein, W.C., Pettijohn, F.C., 1990. Manual of Sedimentary Petrography. SEPM Reprint Series 13, SEPM Society for Sedimentary Geology, Tulsa, Oklahoma, 549 pp.

Lockner, D.A., Byerlee, J.D., 1993. How geometrical constraints contribute to the weakness of mature faults. Nature 363, 250–252.

Main, I.G., Kwon, O., Ngwenya, B.T., Elphick, S.C., 2000. Fault sealing during deformation band growth in sandstones. Geology 28, 1131–1134.

Mair, K., Frye, K.M., Marone, C., 2002. Influence of grain characteristics on the friction of granular shear zones. Journal of Geophysical Research 107, 2219, doi:10.1029/2001JB000516.

Malinverno, A., Ryan, W.B.F., 1986. Extension in the Tyrrhenian Sea and shortening in the Apennines as result of arc migration driven by sinking of the lithosphere. Tectonics 5, 227–254.

Mancini, E.A., Blasingame, T.A., Archer, R., Panetta, B.J., Haynes, C.D., Benson, D.J., 2004. Improving hydrocarbon recovery from mature oil fields producing from carbonate facies through integrated geoscientific and engineering reservoir characterization and modeling studies, Upper Jurassic Smackover Formation, Womack Hill Field (Eastern Gulf Coast, USA). AAPG Bulletin 88, 1629–1651.

Mandl, G., de Jong, L.N.J., Maltha, A., 1977. Shear zones in granular material – an experimental study of their structure and mechanical genesis. Rock Mechanics 9, 95–144.

Marone, C., Scholz, C.H., 1989. Grain-size distribution and microstructures within simulated fault gouge. Journal of Structural Geology 11, 799–814.

Marone, C., Hobbs, B.E., Ord, A., 1992. Coulomb constitutive laws for friction: contrasts in frictional behavior for distributed and localized shear. Pure and Applied Geophysics 139, 195–214.

Micarelli, L., Benedicto, A., Wibberley, C.A.J., 2006. Structural evolution and permeability of normal fault zones in highly porous carbonate rocks. Journal of Structural Geology 28, 1214–1227.

Miller, S.A., Collettini, C., Chiaraluce, L., Cocco, M., Barchi, M., Kaus, B.J.P., 2004. Aftershocks driven by a high-pressure CO_2 source at depth. Nature 427, 724–727.

Morgan, J.K., 1999. Numerical simulations of granular shear zones using the distinct element method. 2. Effects of particle size distribution and interparticle friction on mechanical behavior. Journal of Geophysical Research 104, 2721–2732.

Morgan, J.K., Boettcher, M.S., 1999. Numerical simulations of granular shear zones using the distinct element method. 1. Shear zone kinematics and the micromechanics of localization. Journal of Geophysical Research 104, 2703–2719.

O'Brien, G.S., Bean, C.J., McDermott, F., 2003. A numerical study of passive transport through fault zones. Earth and Planetary Science Letters 214, 633–643.

Poppe, L.J., Eliason, A.H., Fredericks, J.J., Rendigs, R.R., Blackwood, D., Polloni, C.F., 2000. Grain-size analysis of marine sediments: methodology and data processing. U.S Geological Survey Open File Report 00-358, 37.

Prasher, C.L., 1987. Crushing and Grinding Process Handbook. Wiley, New York, 474 pp.

Rawling, G.C., Goodwin, L.B., 2003. Cataclasis and particulate flow in faulted, poorly lithified sediments. Journal of Structural Geology 25, 317–331.

Salvini, F., Billi, A., Wise, D.U., 1999. Strike-slip fault-propagation cleavage in carbonate rocks: the Mattinata Fault zone. Journal of Structural Geology 21, 1731–1749.

Sammis, C.G., King, G., 2007. Mechanical origin of power law scaling in fault zone rock. Geophysical Research Letters 34, L04312, doi:10.1029/2006GL028548.

Sammis, C.G., King, G., Biegel, R., 1987. The kinematics of gouge deformation. Pure and Applied Geophysics 125, 777–812.

Shepherd, R.G., 1989. Correlations of permeability and grain-size. Ground Water 27, 633–638.

Steacy, S.A., Sammis, C.G., 1992. A damage mechanics model for fault zone friction. Journal of Geophysical Research 97, 587–594.

Storti, F., Billi, A., Salvini, F., 2003. Particle size distributions in natural carbonate fault rocks: insights for non-self-similar cataclasis. Earth and Planetary Science Letters 206, 173–186.

Storti, F., Balsamo, F., Salvini, F., 2006. Particle shape and size data from natural granular wear material support non self-similar cataclasis in carbonate fault rocks. Geophysical Research Abstracts 8, 2560.

Vittori, E., Cavinato, G.P., Miccadei, E., Rughi, D., Serva, L., 1991. First results of a study on cataclastic and intense fracturing processes in calcareous rocks (Central Apennines, Italy). Bollettino della Società Geologica Italiana 110, 489–499.

Wibberley, C.A.J., Shimamoto, T., 2003. Internal structure and permeability of major strike-slip fault zones: the Median Tectonic Line in Mie Prefecture, Southwest Japan. Journal of Structural Geology 25, 59–78.

Wilson, B., Dewers, T., Reches, Z., Brune, J., 2005. Particle size and energetics of gouge from earthquake rupture zones. Nature 434, 749–752.

Wilson, J.E., Goodwin, L.B., Lewis, C., 2006. Diagenesis of deformation band faults: record and mechanical consequences of vadose zone flow and transport in the Bandelier Tuff, Los Alamos, New Mexico. Journal of Geophysical Research 111, B09201, doi:10.1029/2005JB003892.